



This is a repository copy of *Enhanced dynamic control strategy for stacked dynamic regulation frequency response services in battery energy storage systems*.

White Rose Research Online URL for this paper:

<https://eprints.whiterose.ac.uk/206454/>

Version: Published Version

Article:

Ahmouda, A. and Gladwin, D.T. orcid.org/0000-0001-7195-5435 (2023) Enhanced dynamic control strategy for stacked dynamic regulation frequency response services in battery energy storage systems. *Energies*, 16 (23). 7686. ISSN 1996-1073

<https://doi.org/10.3390/en16237686>

Reuse

This article is distributed under the terms of the Creative Commons Attribution (CC BY) licence. This licence allows you to distribute, remix, tweak, and build upon the work, even commercially, as long as you credit the authors for the original work. More information and the full terms of the licence here:

<https://creativecommons.org/licenses/>

Takedown


If you consider content in White Rose Research Online to be in breach of UK law, please notify us by emailing eprints@whiterose.ac.uk including the URL of the record and the reason for the withdrawal request.



eprints@whiterose.ac.uk
<https://eprints.whiterose.ac.uk/>

Article

Enhanced Dynamic Control Strategy for Stacked Dynamic Regulation Frequency Response Services in Battery Energy Storage Systems

Abdulkarim Ahmouda [†] and Daniel T. Gladwin ^{*,†} 

Department of Electronic and Electrical Engineering, University of Sheffield, Sheffield S10 2TN, UK; aaahmouda1@sheffield.ac.uk

* Correspondence: d.gladwin@sheffield.ac.uk

† These authors contributed equally to this work.

Abstract: Energy storage systems are undergoing a transformative role in the electrical grid, driven by the introduction of innovative frequency response services by system operators to unlock their full potential. However, the limited energy storage capacity of these systems necessitates the development of sophisticated energy management strategies. This paper investigates the newly introduced frequency response service, Dynamic Regulation, within the Great Britain electrical grid. Our study not only establishes control parameters but also demonstrates a novel approach to energy management that pushes the boundaries of the allowable service envelope. We present two distinctive control methods, the first serving as a reference for standard response, and the second as a dynamic control approach, exploiting the extremities of the allowable service envelope. A comprehensive sensitivity analysis that considers availability, the number of equivalent full cycles, and cost–revenue analysis based on grouped dynamic control state of charge setpoints is carried out. Our results underscore that the optimization of average availability takes precedence over merely minimizing the number of cycles, which leads us to define a target state of charge range of between 40% and 45% for a 1-h battery to achieve an availability >95%. Furthermore, our study presents simulated results utilizing real-world frequency data, which reveal the transformative potential of the latter control method. By enhancing the availability of battery energy storage systems, this innovative approach promises not only higher revenues for the asset owner but also assists the system operator in managing frequency.

Keywords: energy storage system; dynamic regulation; energy management; frequency response; dynamic control



Citation: Ahmouda, A.; Gladwin, D.T. Enhanced Dynamic Control Strategy for Stacked Dynamic Regulation Frequency Response Services in Battery Energy Storage Systems. *Energies* **2023**, *16*, 7686. <https://doi.org/10.3390/en16237686>

Academic Editor: JongHoon Kim

Received: 25 September 2023

Revised: 13 November 2023

Accepted: 16 November 2023

Published: 21 November 2023



Copyright: © 2023 by the authors. Licensee MDPI, Basel, Switzerland. This article is an open access article distributed under the terms and conditions of the Creative Commons Attribution (CC BY) license (<https://creativecommons.org/licenses/by/4.0/>).

1. Introduction

The increase in the integration level of variable renewable energy resources (RES), such as wind and solar, into the power grid in the form of distributed generation (DG) has driven global efforts to reduce greenhouse gas emissions [1,2]. These resources are considered as variable, independent, and intermittent by nature and can contribute to power quality, stability, and reliability issues [3,4]. To mitigate these problems, excess energy can be stored when generation exceeds demand and then this stored energy can be used when demand exceeds supply such as at peak times [5]. Grid-connected Energy Storage Systems (ESSs) are widely regarded as an enabler for RES [6–8]. The stored energy can be used to improve power quality as well as to achieve better grid performance. In addition, energy storage can be used to mitigate energy security issues that result from intermittent renewable power. This will lead to a better contribution in the prediction response of such resources, while, at the same time, providing additional flexibility in the energy system [9]. Integration of ESSs with the grid will enable the large-scale expansion of RES and lead to a faster transition to a low-carbon future energy system [10,11]. ESSs can be realized

using different technologies, which include battery, flywheel, pumped-storage hydropower, supercapacitor, compressed air, hydrogen, and thermal (including molten salt). There are many features of ESSs that relate to its electrical capacity, efficiency, charge/discharge behaviour, lifetime, cost, and environmental/location issues. Some of these characteristics are intimately related to each other [1]. The operational capabilities of ESS types are, therefore, significantly different, with some being suitable to mitigate annual fluctuations, while others could be ideally used for very short peak power requirements [10,12,13]. Pumped hydroelectric storage (PHS) is considered the most widely deployed energy storage technology to date; however, this type of ESS is constrained by geographical limitations [14]. In [15], battery energy storage systems (BESSs) have been successfully demonstrated in grid applications to provide power-balancing services. BESSs are considered favorable because they have several advantages, which include high energy efficiency, good energy density, variable charging/discharging rates, faster response time compared to conventional energy generation sources, low self-discharge rates, and low maintenance [16]. One commonly quoted use for a BESS is to provide ancillary services that are used to balance demand and supply; these include fast frequency response services, voltage support, and peak power lopping [17]. In addition, in recent years, the cost of battery cells has declined, and this has led to increased profitability of BESSs for large-scale grid applications [18]. In Great Britain (GB), in order to maintain frequency very close to 50 Hz, the National Grid Electricity System Operator (NGESO)—the primary electricity system network operator—has introduced various frequency response services to provide a real-time response to deviations in the grid frequency, and they include Enhanced Frequency Response (EFR), Dynamic Firm Frequency Response (DFR) and Static Firm Frequency Response (SFR), and new frequency response services, which include Dynamic Contaminant (DC), Dynamic Regulation (DR), and Dynamic Moderation (DM) [19–21]. In this paper, one of the new frequency response services, DR, which contains two service conditions, Dynamic Regulation High-Frequency Response (DR-HF) and Dynamic Regulation Low-Frequency Response (DR-LF), has been modeled in MATLAB/Simulink using a generalized ESS and simulated against a real-world frequency data set obtained from NGESO [22]. The paper investigates whether the allowable limits, as defined by NGESO, for the delivery parameters of the service could be exploited to manage the state of charge (SOC) of the BESS using a dynamic control strategy to achieve higher availability. This control offers either a fast or slow response to changes in frequency to minimize energy throughput. The service error calculation for contracted delivery is presented and used to demonstrate increased revenue through dynamic control. Two scenarios are investigated for comparison. The first scenario (S1) is a base case, where a stacked DR-HF and DR-LF service has been delivered without implementing the dynamic control. For the second scenario (S2), both services have been delivered using the dynamic control to assist with SOC management. To conclude, a sensitivity analysis is carried out to assess a stacked DR-HF and DR-LF service in terms of energy throughput, availability, penalty payment, and number of equivalent full cycles (EFCs).

2. Dynamic Regulation (DR)

DR is considered a pre-fault service that is designed to slowly correct continuous but small deviations in frequency. The DR contains two service conditions: Dynamic Regulation High-Frequency Response (DR-HF) and Dynamic Regulation Low-Frequency Response (DR-LF). The aim of such a service is to continually regulate frequency around the target of 50 Hz. In order to comply with the NGESO specifications, as shown in Table 1, an ESS must continually respond to the grid frequency deviation through increased or decreased import/export power. In this service, the deadband (DB) is considered as the area that is limited by frequency band ± 0.015 Hz. For both DR-LF and DR-HF, there is no requirement to import/export power in the DB, but there is also no opportunity to charge/discharge the ESS to manage its SOC. From the edge of the DB to -0.2 Hz for DR-LF or $+0.2$ Hz for DR-HF, the DR power demand (P_{DR}) increases linearly to 100% of the contracted quantity. According to NGESO specifications, actual BESS power (P_{BESS}) needs to start

responding to changes in P_{DR} within 2 s and must deliver the full P_{DR} no later than 10 s [23].

DR Service Specification

Table 1. Service specification of DR service model [23].

Parameter	Values	Unites
Deadband (delivery %)	± 0.015	Hz
Delivery range	± 0.015 to ± 0.2	Hz
Initial linear range (delivery %)	± 0.015 to ± 0.2 (100% at ± 0.2)	Hz
Full delivery point	± 0.2	Hz
Max time to full delivery	10	s
Ramp time	8	s
Max ramp start	2	s
Delivery duration	1	h

Figure 1 illustrates a high-level block diagram of the DR model (DR-LF, DR-HF, or both services) as used in MATLAB/Simulink. The first block represents the real-time grid frequency (f) with a unit (Hz) that changes second by second and has been obtained from the national grid (NG) [22]. The grid frequency is input into the second block, called a service power calculation block, that calculates P_{DR} for the required frequency response service (DR-LF or DR-HF) or both services. The calculation of P_{DR} is demonstrated in Table 2, where the required P_{DR} envelope is calculated as a function of the desired limits according to NG specifications. The obtained P_{DR} is measured in watts (W) and then converted to kilowatts (kW). It is also possible to convert the power unit to per unit (p.u), where 40 MW is equal to 1 p.u.

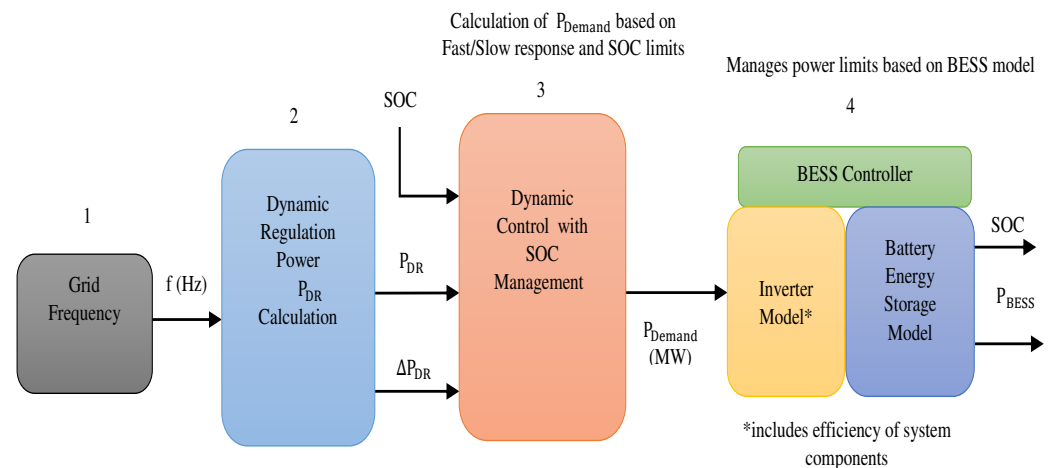


Figure 1. Block diagram of DR Service model.

Table 2. P_{DR} and frequency setpoints and calculations in the control algorithm.

Freq. (Hz)	Contracted Power (p.u)	P_{DR} (p.u)
J = 49.5	$j = 1$	$P_{DR} = j$
K = 49.8	$k = 1$	$P_{DR} = k$
L = 49.985	$l = 0$	$P_{DR} = [(\frac{L-f}{L-K}) \times (k - l) + l]$
M = 50	$m = 0$	$P_{DR} = 0$
N = 50.015	$n = 0$	$P_{DR} = [(\frac{O-f}{O-N}) \times (n - o) + o]$
O = 50.2	$o = -1$	$P_{DR} = o$
P = 50.5	$p = -1$	$P_{DR} = p$

Table 2 and Figure 2 show the algorithm for the proposed model, which starts by detecting the position of the measured frequency in relation to the zones bounded by frequency values 'J' to 'P', as shown in Table 2. The P_{DR} setpoint can be calculated using the appropriate equation to give $P_{DR(LF\ or\ HF)}$ or both services. According to NGENSO [23], P_{BESS} must be delivered as per the service envelope specification as previously described; if the power is delivered outside the agreed range, this will then cause a reduction in a metric called the Service Performance Measurement (SPM), resulting in a reduced payment for the contracted service. Contractual obligations require that power delivered to the grid is recorded at 20 Hz and must be provided as evidence of this operation to NGENSO for the SPM to be calculated. In the DB, the required $P_{DR} = 0$.

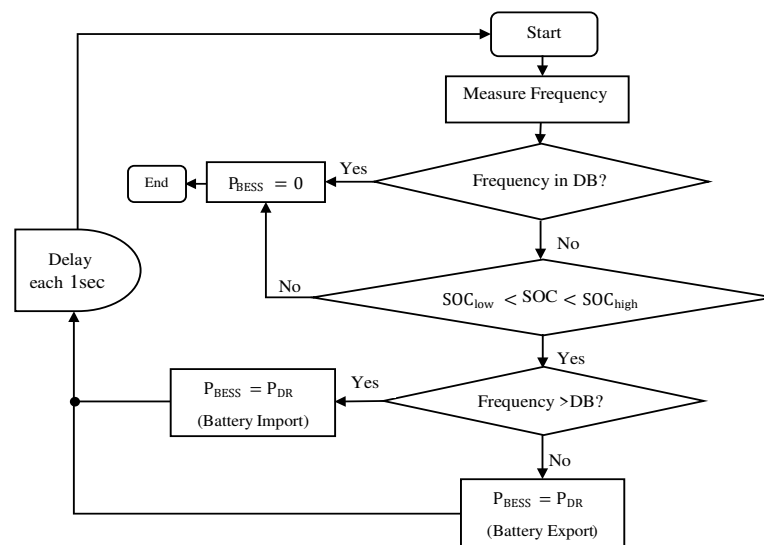


Figure 2. Implemented BESS power management strategy for DR service model.

The third block represents the dynamic control with SOC management, where the three inputs are included; SOC, power calculations $P_{DR(LF\ or\ HF)}$ or for both services, and $\Delta P_{DR(LF\ or\ HF)}$ or for both services, while the output is the required P_{Demand} , which is connected to the BESS block through the inverter, as illustrated in Figure 1. Figure 3 shows the implementation of dynamic control of the DR service model.

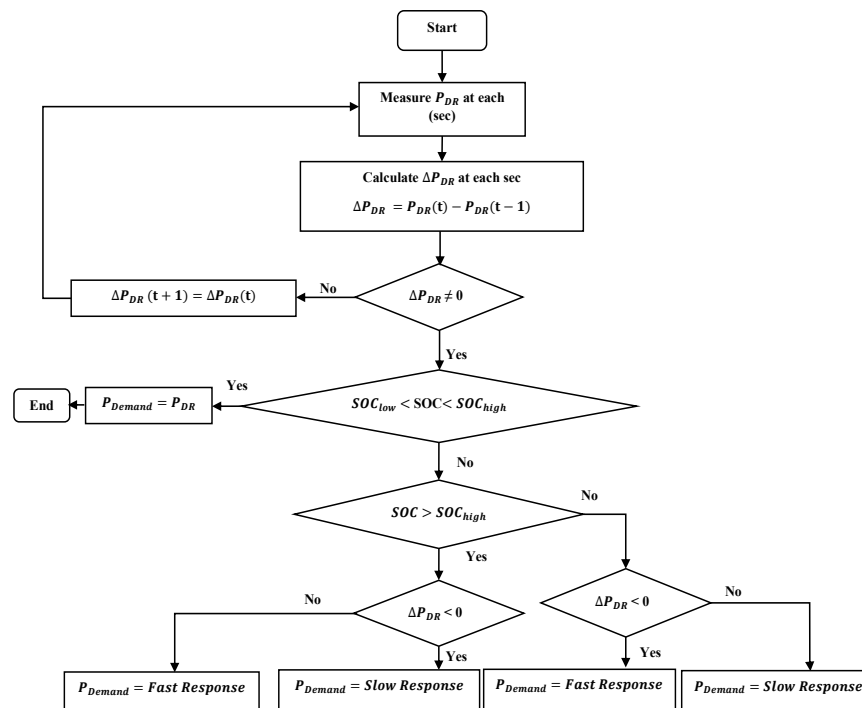


Figure 3. Flow diagram of Dynamic Control Model.

As we can see from Figure 3, the algorithm starts to measure P_{DR} each second then calculates the ΔP_{DR} ; this is based on the desired SOC limitations. Thus, if ΔP_{DR} is equal to zero then the current ΔP_{DR} will be equal to the previous ΔP_{DR} . Whereas, if ΔP_{DR} is negative or positive and SOC is in between the agreed limits, then P_{Demand} will equal to the contracted power (P_{DR}). However, if SOC is greater than SOC_{high} and ΔP_{DR} is less than zero, then the slow response will be implemented, while, if ΔP_{DR} is greater than zero, then the fast response will be implemented (and vice versa in the case where SOC is less than SOC_{low}).

The final blocks consist of an inverter and a battery energy storage model, both controlled by a BESS controller. The input to this controller is the dynamic control output, P_{Demand} . The BESS controller manages the power delivered by the BESS based on P_{Demand} , while adhering to any power and SOC limits. These SOC limits are defined as $SOC_{low} = 5\%$ and $SOC_{high} = 95\%$. Consequently, if the battery's SOC reaches either the upper or lower limit, it will cease importing or exporting power. The SOC of the BESS is calculated, as described in [15], using the following equation:

$$SOC_{end} = SOC_{start} + \frac{\int_0^t P_{BESS} dt}{3600 \cdot Q} \quad (1)$$

where SOC_{start} , Q and P_{BESS} represent initial SOC, Watt-hour capacity, and instantaneous P_{BESS} , respectively.

Also, in this block, the stored energy in the BESS has been calculated using a switch, where the input is the P_{Demand} , which is the output power of the third block calculated, multiplied by the charge/discharge efficiency. The calculation of Stored Energy in the BESS, as in [19], is expressed in the following equations:

$$E_t = - \int_0^t \frac{P_t}{\eta_D} .dt \quad (2)$$

$$E_t = - \int_0^t P_t \cdot \eta_C .dt \quad (3)$$

where η_D , η_C , P_t , and E_t refer to the battery discharge efficiency, battery charge efficiency, battery power for charging or discharging at a specific hour (t), and stored energy in the battery at that hour (t). It is important to note that, if $P_t > 0$ is positive, indicating that the system is exporting or discharging, Equation (2) can be used, whereas, if P_t is negative, indicating that the system is importing or charging, Equation (3) can be used.

2.1. DR-LF or DR-HF Service Envelope

Figures 4 and 5 show the relationship between P_{DR} and the frequency data for DR-LF and DR-HF service, respectively. In these services, the assets must respond to low or high-frequency events by exporting and importing power.

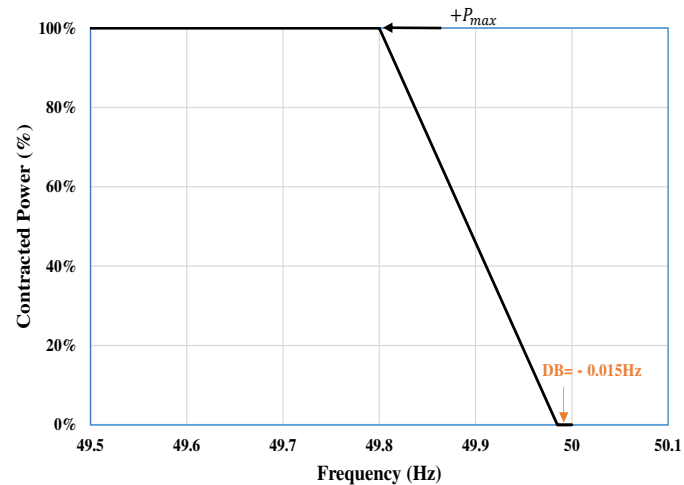


Figure 4. Power vs. frequency for DR-LF service.

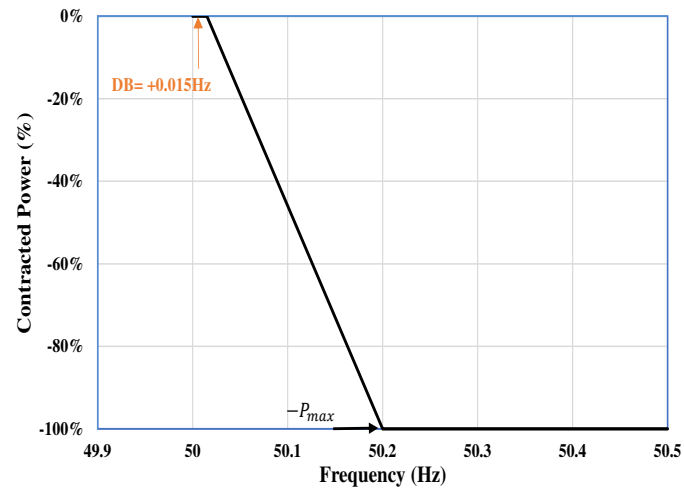


Figure 5. Power vs. frequency for DR-HF service.

2.2. DR-LF and DR-HF Service Envelope

Figure 6 illustrates the relationship between frequency data obtained from NG and P_{DR} for stacked DR-LF and DR-HF. In this service, the assets must respond to both low- and high-frequency events by exporting and importing power. The parameters used in the DR model are shown in Table 3.

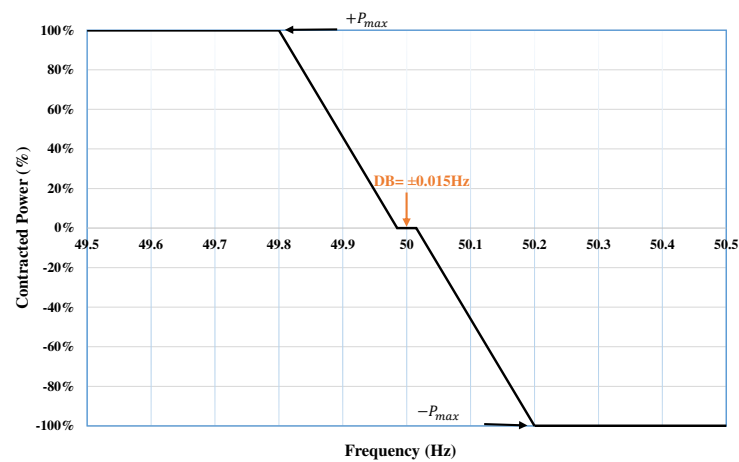


Figure 6. Power vs. frequency for DR-HF and DR-LF service.

Table 3. DR model parameters.

Parameters	Values
Nominal Grid Frequency	50 Hz
DeadBand (DB)	± 0.015 Hz
Battery initial (SOC_{init})	50%
Battery charge/discharge efficiency	97% [24,25]
Inverter efficiency	97% [24,25]
Battery Power/Energy	40 MW/40 MWh
Dynamic control SOC setpoints (SOC_{low} & SOC_{high})	40–45%

2.3. Simulation Results of DR-HF Service Model

Figure 7 depicts the simulation results of a BESS delivering Demand Response with DR-HF, contracted for 40 MW, for the first 18 h of January 2019. The plots include data for frequency, P_{Demand} , P_{BESS} , and SOC. The blue dashed lines on the frequency plot represent the DB (± 0.015 Hz). The P_{Demand} and P_{BESS} are represented by orange and violet colors, respectively.

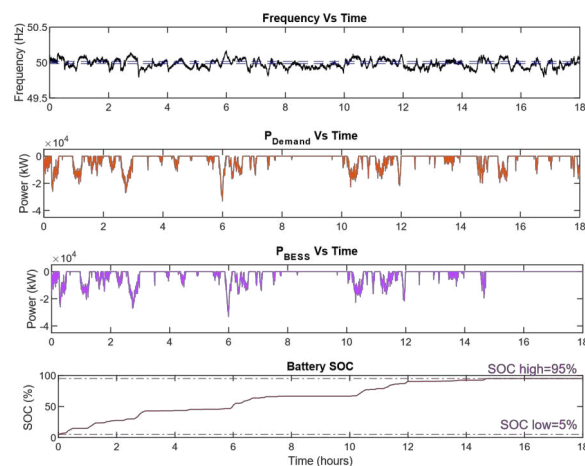


Figure 7. Simulation results of DR-HF service for the first 18 h on January 2019 (40 MW/40 MWh ESS).

In this section, SOC_{start} has been set to 5%, and the SOC limits for the BESS are indicated on the SOC plot by purple dashed lines: $SOC_{high} = 95\%$ and $SOC_{low} = 5\%$. It is evident that SOC_{high} is not breached in the simulation. If the BESS reaches the upper limit, as it does at 14.7 h, then the system can only export power, and P_{BESS} will be set to zero.

2.4. Simulation Results of DR-LF Service Model

Figure 8 presents the simulation results of a BESS delivering DR-LF, contracted for 40 MW, for the first 9 h on January 2019 for frequency, P_{Demand} , P_{BESS} , and SOC. The plots include data for frequency, P_{Demand} , P_{BESS} , and SOC. The purple dashed lines on the frequency plot represent the DB (± 0.015 Hz). The P_{Demand} and P_{BESS} are represented by orange and blue colors, respectively.

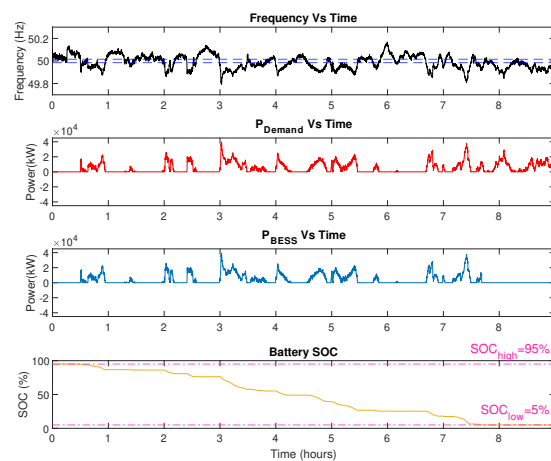


Figure 8. Simulation Results of DR-LF Service for first 9 h on January 2019 (40 MW / 40 MWh ESS).

In this section, the SOC_{start} has been set to 95%, and SOC limits for the BESS are indicated on the SOC plot by pink dashed lines and set as the same values as in DR-HF; it is clear that SOC_{low} is not breached in the simulation. If the BESS reaches this limit, as it does at 7.4 h, then the system can only import power and P_{BESS} will be set to zero.

2.5. Simulation Results of Both DR-HF and DR-LF Services

Figure 9 presents the simulation results of a BESS delivering DR-HF and DR-LF, contracted for 40 MW, for the first 3 days of January 2019 for frequency, P_{Demand} , P_{BESS} , and SOC. The blue dashed lines on the frequency plot represent the DB (± 0.015 Hz). The P_{Demand} and P_{BESS} are represented by red and blue colors, respectively.

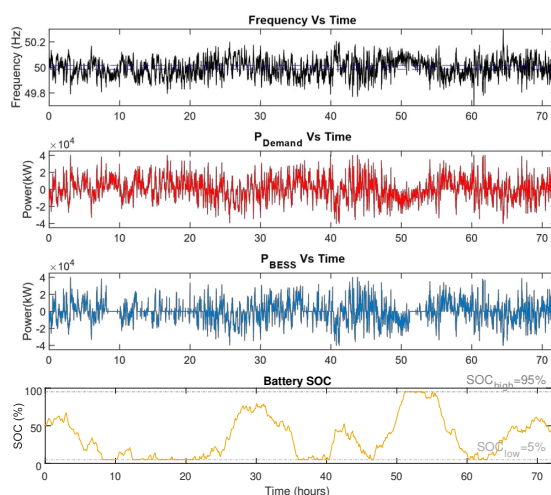


Figure 9. Simulation results of DR-HF and DR-LF Services for the first 3 days of January 2019 (40 MW / 40 MWh BESS).

In this section, SOC_{start} has been set to 50%, and the SOC limits for the BESS are indicated on the SOC plot by grey dashed lines: $SOC_{high} = 95\%$ and $SOC_{low} = 5\%$. It can be seen that P_{Demand} and P_{BESS} are changing proportionally with change in the frequency data that are obtained from NG [22] second by second, and the deadband (DB) is shown with the limits (± 0.015 Hz); in this area, there is no opportunity for BESS to manage SOC, which means power is equal to zero. Also, it shows both SOC_{high} and SOC_{low} are not breached in the simulation. If the BESS reaches a higher limit, as is shown in this figure, then the system can only export power and BESS will be set to zero, whereas, if the BESS reaches the lower limit, as it does in this figure, then the system can only import power and P_{BESS} will be set to zero.

2.6. Dynamic Control of DR-LF or DR-HF

The objective of implementing the dynamic control is that there is an opportunity to exploit the speed of the control response to assist with SOC management as there is no opportunity in the DB. In this section, we consider the ESS delivering either DR-LF or DR-HF and do not consider the case of delivering both in a stacked bid [23]. The strategy in this work is to minimize the energy throughput for either service by responding quickly to decreases in P_{DR} and slowly to increases in P_{DR} , the sign of which depends on the service being delivered. The fast response will use a 100% p.u./s ramp rate for P_{Demand} , resulting in the power being delivered within 1 s. The slow response follows the slower limits of the service specification, in that P_{DR} must be delivered no later than 10 s, with a minimum delay period of 2 s. This is implemented using a fixed control delay of 2 s and a ramp rate of 12.5% p.u./s.

2.6.1. Dynamic Control of DR-HF

For DR-HF delivery, the SOC_{start} will be set at the lower limit ($SOC_{low} = 5\%$). The fast response will be delivered if the change in DR-HF power $\Delta P_{(DR-HF)} > 0$, whereas the slow response is implemented if $\Delta P_{(DR-HF)} < 0$.

Figure 10 shows the simulation results of DR-HF for both fast and slow responses by using an illustrative example input which represents $P_{(DR-HF)}$. It can be seen that, when $P_{(DR-HF)}$ increases ($\Delta P_{(DR-HF)} < 0$), then the slow control response is applied, whereas, when ($\Delta P_{(DR-HF)} > 0$), then a fast response is used. In this methodology for DR-HF, the control is switching between ramp rates and uses the maximum allowable delay to minimize the charging power.

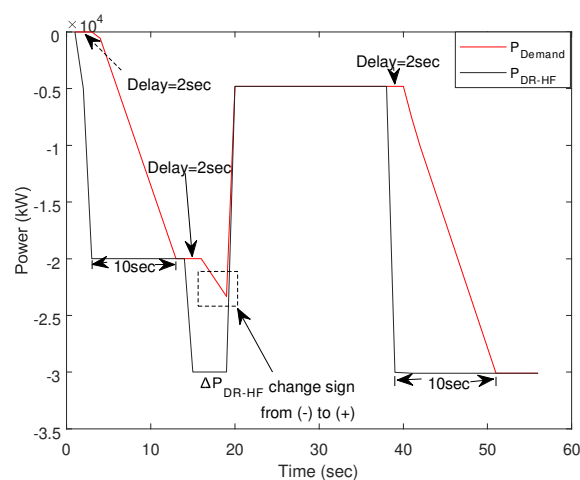


Figure 10. Simulation results of DR-HF with Dynamic Control using test inputs.

2.6.2. Dynamic Control of DR-LF

For DR-LF, the SOC_{start} will be set at a higher limit ($SOC_{high} = 95\%$). The fast response will be delivered if the change in DR-LF power $\Delta P_{(DR-LF)} < 0$, whereas a slow response could be implemented if $\Delta P_{(DR-LF)} > 0$.

Figure 11 illustrates the simulation results of DR-LF for both fast and slow responses again by using an illustrative example that represents $P_{(DR-LF)}$. It can be seen that, when $P_{(DR-LF)}$ increases ($\Delta P_{(DR-LF)} > 0$), a slow control response is applied; when ($\Delta P_{(DR-LF)} < 0$), then the fast response is used. For DR-LF, this means that the discharging power is minimized. The result is that, for both DR-HF and DR-LF, the energy throughput is minimized over the service delivery with the aim of extending the time before the SOC limits are reached.

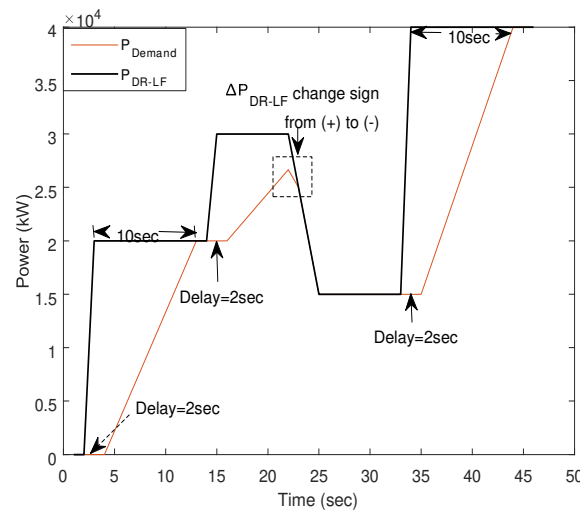


Figure 11. Simulation results of DR-LF with Dynamic Control using test inputs.

2.7. BESS Availability

In this work, the availability of the BESS is defined as the percentage of time that it can deliver P_{Demand} ; it is considered unavailable when the SOC is at its limit and, therefore, unable to deliver P_{Demand} . The availability of BESS can be calculated using Equation (4) [26]:

$$Availability = \left(1 - \frac{(Non - available\ BESS\ time)}{(Total\ simulation\ time)}\right) \times 100 \tag{4}$$

In the results, 'avg. Availability' is presented; this is the average value of the BESS Availability for each month and includes the BESS being available when the $P_{Demand} = 0$.

2.8. Number of Equivalent Full Cycles (EFCs)

In this paper, a method is used to calculate the number of Equivalent Full Cycles (EFCs) required to deliver a service over a time period. This is particularly important for a BESS, as the system will degrade (reduced capacity, for example) with increased cycles; Ref. [27] states that, in commercial documents such as warranties, an EFC is calculated using energy throughput, as shown in Equation (5):

$$EFCs = \frac{Total\ of\ Export\ and\ Import\ Energy\ of\ ESS}{Total\ Energy\ throughput\ by\ Capacity} / 2 \tag{5}$$

2.9. Penalty Payment

To define load profiles through the day, there are six Electricity Forward Agreement (EFA) blocks in 24 h, and each EFA block represents 4 h of the day [28]. These are the minimum units of time an ESS can bid to deliver a service. Each half-hour period of the day is referred to as the Settlement Period (SP) and is used as a time unit for the purposes of

energy trading and balancing. To calculate the penalty payment for the service, we need to define the upper and lower bounds of the service. Based on the scenarios presented in this paper, these correlate with the fast ($P_{DR(upper)}$) and slow ($P_{DR(lower)}$) control response. If the P_{BESS} is on or between these bounds, then the error is calculated as zero. However, if P_{BESS} is outside of these bounds, then the error can be calculated by taking the difference between P_{BESS} and the upper or lower bounds [22,29]. The error e_m for one-time measurement and metered response (P_{BESS}) can be calculated using Equation (6) and implemented as shown in Figure 12.

$$e_m = \left\{ \begin{array}{ll} P_{DR(lower)} - P_{BESS} & P_{BESS} < P_{DR(lower)} \\ 0 & P_{DR(lower)} \leq P_{BESS} \leq P_{DR(upper)} \\ P_{BESS} - P_{DR(upper)} & P_{BESS} > P_{DR(upper)} \end{array} \right\} \quad (6)$$

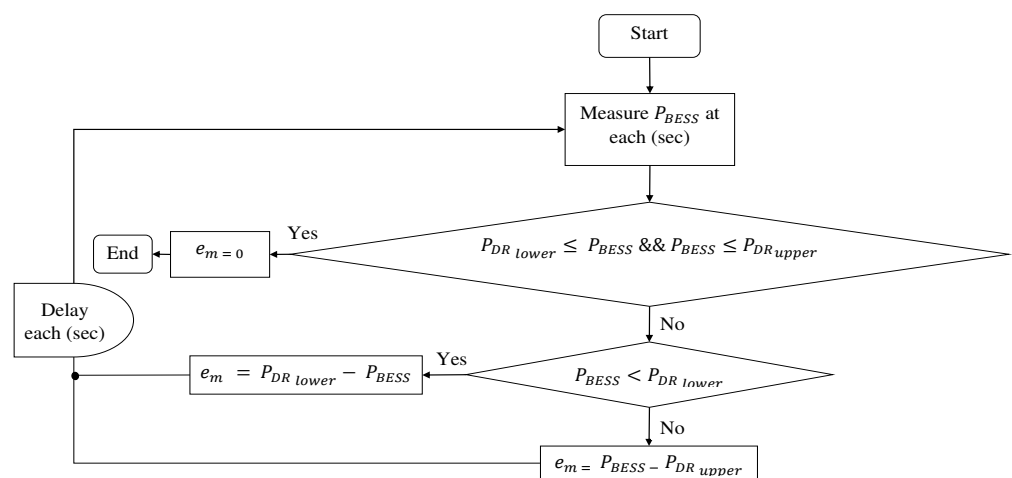


Figure 12. Implemented error calculation (e_m) for DR service model.

The scaled error (es_m) for one measurement is given by

$$es_m = \frac{e_m}{P_{contract}} \quad (7)$$

where e_m is the calculated error and $P_{contract}$ is the contracted quantity that the provider is contracted to deliver; in this work, the example is 40 MW. For each settlement period (SP), the performance score can be calculated using

$$E = \max_m \left(\text{rolling_mean}_{\text{over 2 seconds}} es_m \right) \quad (8)$$

and the factor for each SP can be calculated as shown in Equation (9):

$$K_j = \left\{ \begin{array}{ll} 1 & E < A \\ 1 - \frac{E-A}{B-A} & A \leq E \leq B \\ 0 & E > B \end{array} \right\} \quad (9)$$

where $A = 0.03$ and $B = 0.07$. For each contracted EFA block, the K_e factor can be calculated as shown in Equation (10):

$$K_e = \min_j K_j \quad (10)$$

The payment adjustment (K_e factor) curve is shown in Figure 13.

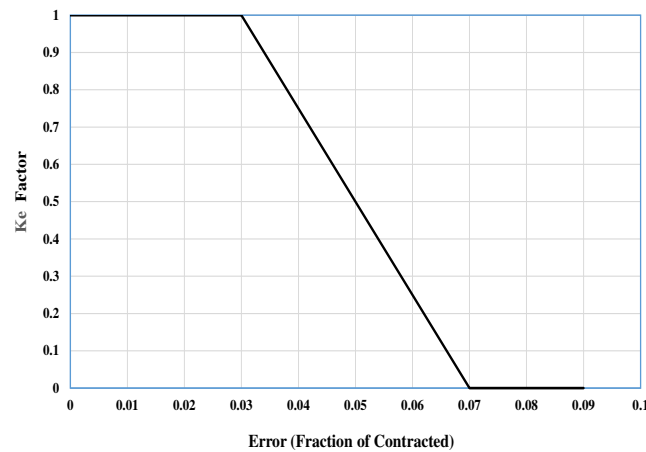


Figure 13. The payment adjustment (K_e factor) curve.

2.10. Dynamic Control of DR-LF and DR-HF

In this section, BESS has been procured for staking DR-LF and DR-HF services. The SOC_{start} is set at 50%, and fast and slow responses are delivered based on the dynamic control SOC_{higher} & SOC_{lower} setpoints. Therefore, four steps are taken into account:

1. For DR-LF delivery, the slow response will be delivered if $(\Delta P_{DR(t-1)} > 0)$ && $(\Delta P_{DR(t)} > 0)$ && $(SOC < SOC_{lower})$, whereas the fast response is implemented if $(\Delta P_{DR(t-1)} < 0)$ && $(\Delta P_{DR(t)} < 0)$ && $(SOC < SOC_{lower})$, and the results are shown in Figure 10. Figure 10 illustrates the simulation results of DR-LF for both fast and slow responses again by using an illustrative example, which represents $P_{(DR-LF)}$ when $(SOC < SOC_{lower})$. It can be seen that, when $P_{(DR-LF)}$ increases ($P_{DR-LF(t-1)} > 0$) && $(\Delta P_{DR-LF(t)} > 0)$, a slow control response is applied; when $(P_{DR-LF(t-1)} < 0)$ && $(\Delta P_{DR-LF(t)} < 0)$, then the fast response is used. For DR-LF, this means that the discharging power is minimized;
2. For DR-HF delivery, the slow response will be delivered if $(\Delta P_{DR(t-1)} > 0)$ && $(\Delta P_{DR(t)} > 0)$ && $(SOC < SOC_{lower})$, whereas the fast response is implemented if $(\Delta P_{DR(t-1)} < 0)$ && $(\Delta P_{DR(t)} < 0)$ && $(SOC < SOC_{lower})$, and the results are shown in Figure 14. Figure 14 presents the simulation results of DR-HF for both fast and slow responses by using an illustrative example input which represents the $P_{(DR-HF)}$ when $SOC < SOC_{lower}$. It can be noticed that, when $P_{(DR-HF)}$ decreases, which means $(P_{DR-HF(t-1)} > 0)$ && $(\Delta P_{DR-HF(t)} > 0)$, a slow control response is applied, while, when $(P_{DR-HF(t-1)} < 0)$ and $(\Delta P_{DR-HF(t)} < 0)$, then the fast control response is applied. The aim of this methodology for DR-HF control is switching between ramp rates and using the maximum allowable delay to minimize the discharging power when $SOC < SOC_{lower}$;
3. For DR-HF delivery, the slow response will be delivered if $(\Delta P_{DR(t-1)} < 0)$ && $(\Delta P_{DR(t)} < 0)$ && $(SOC > SOC_{higher})$, whereas the fast response is implemented if $(\Delta P_{DR(t-1)} > 0)$ && $(\Delta P_{DR(t)} > 0)$ && $(SOC > SOC_{higher})$, and the results are shown in Figure 11. Figure 11 shows the simulation results of DR-HF for both fast and slow responses by using an illustrative example input, which represents $P_{(DR-HF)}$. It can be seen that, when $P_{(DR-HF)}$ increases ($\Delta P_{(DR-HF)} < 0$), then the slow control response is applied, whereas, when $(\Delta P_{(DR-HF)} > 0)$, then a fast response is used. In this methodology, the target of the dynamic control for DR-HF is to be used to minimize the charging power when $SOC > SOC_{higher}$;
4. For DR-LF delivery, the slow response will be delivered if $(\Delta P_{DR(t-1)} < 0)$ && $(\Delta P_{DR(t)} \leq 0)$ && $(SOC > SOC_{higher})$, whereas the fast response is implemented if $(\Delta P_{DR(t-1)} > 0)$ && $(\Delta P_{DR(t)} > 0)$ && $(SOC > SOC_{higher})$, and the results are shown in Figure 15.

Figure 15 illustrates the simulation results of DR-LF for both fast and slow responses by using an illustrative example input, which represents $P_{(DR-LF)}$ when $SOC > SOC_{higher}$. It is clear that, when $P_{(DR-LF)}$ increases ($\Delta P_{(DR-HF)} > 0$), then the fast control response is implemented, whereas, when ($\Delta P_{(DR-LF)} < 0$), then a slow response is used. The aim of this methodology is to exploit the dynamic control for DR-HF to minimize the charging power when $SOC > SOC_{higher}$.

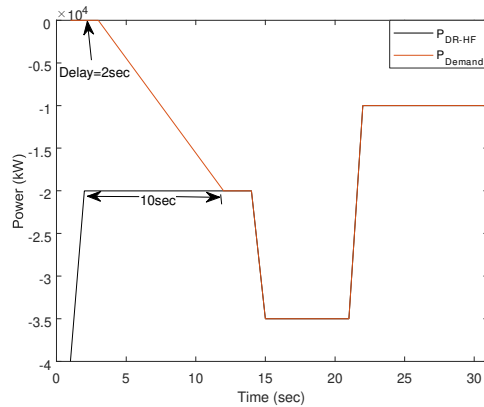


Figure 14. Simulation results of DR-HF with Dynamic Control ($SOC < SOC_{lower}$) using test inputs.

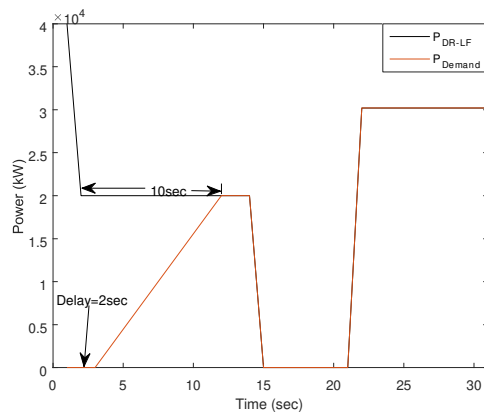


Figure 15. Simulation results of DR-LF with Dynamic Control ($SOC > SOC_{higher}$) using test inputs.

2.11. Analysis of the Availability of BESS Used to Deliver DR-LF and DR-HF Services Based on Grouped Dynamic Control SOC Setpoints

In this section, BESS availability has been calculated using Equation (4) in Section 2.7 and based on grouped dynamic control SOC setpoints (SOC_{higher}) and (SOC_{lower}), in order to select the optimum range of dynamic control SOC setpoints which will have high average availability. The SOC_{lower} grouped as (10%, 15%, 20%, 25%, 30%, 35%, 40%, 45%, 50%), while SOC_{higher} grouped as (45%, 50%, 55%, 60%, 65%, 70%, 75%, 80%, 85%, 90%), and the results are shown in Table 4 and Figure 16.

Table 4. Simulation results of average availability of BESS used to deliver DR-HF and DR-LF services based on a group of dynamic control SOC setpoints for the first 6 EFA blocks for November 2019 frequency data.

	$SOC_{lower}(\%)$								
	10	15	20	25	30	35	40	45	50
$SOC_{higher}(\%)$ 90	89.3809	89.4055	89.4310	89.4672	89.5051	89.5385	89.5595	89.5104	89.4488
85	89.4645	89.4891	89.5139	89.5506	89.5886	89.6213	89.6340	89.5894	89.5467
80	89.5540	89.5785	89.6033	89.6419	89.6799	89.7126	89.7218	89.6599	89.6129
75	89.5954	89.6192	89.6439	89.6816	89.7198	89.7527	89.7660	89.7096	89.6643
70	89.6889	89.7127	89.7381	89.7759	89.8138	89.8471	89.8561	89.7783	89.7163
65	89.7163	89.7400	89.7647	89.8039	89.8430	89.8751	89.8886	89.8072	89.7469
60	89.7472	89.7711	89.7965	89.8342	89.8722	89.9050	89.9159	89.8374	89.7955
55	89.9423	89.9626	89.9882	90.0252	90.0638	90.0963	90.0764	89.9693	89.9060
50	90.2584	90.2813	90.3090	90.3458	90.3913	90.4154	90.4177	90.0893	90.0007
45	90.3262	90.3499	90.3775	90.4144	90.4607	90.4848	90.4879	90.1967	90.1967

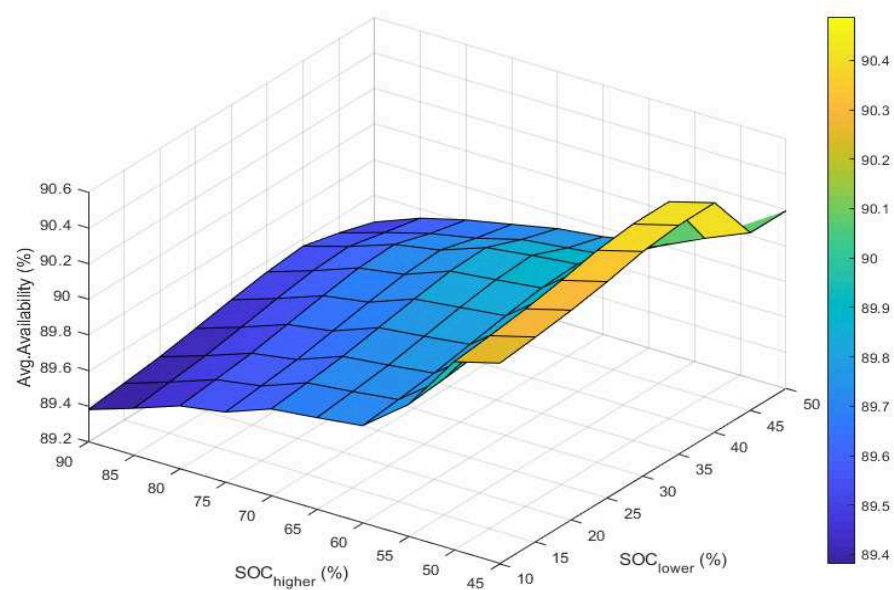


Figure 16. Simulation results of BESS used to deliver DR-HF and DR-LF with dynamic control for the first 6 EFA blocks for December 2019 frequency data (Avg. availability vs. Dynamic Control SOC setpoint).

From Table 4 and Figure 16, it is clear that, from 10–40% SOC_{lower} range and at all ranges of SOC_{higher} , the average availability increases by the increase in SOC_{lower} and with the decrease in SOC_{higher} , and vice versa. The highest value of average availability was at 45% SOC_{higher} and 40% SOC_{lower} , with a value equaling $\sim 90.49\%$. However, when $SOC_{lower} > 40\%$ at all ranges of SOC_{higher} , the average availability was decreased gradually compared to SOC_{lower} when it was equal to 40%. Therefore, the suitable range of dynamic control SOC setpoint is 40% SOC_{lower} –45% SOC_{higher} .

2.12. Analysis of the EFCs of BESS Used to Deliver DR-LF and DR-HF Services Based on a Grouped Dynamic Control SOC Setpoints

In this section, the number of cycles has been obtained from the EFCs counting method using Equation (5) and based on grouped dynamic control SOC setpoints, which are demonstrated in Section 2.11, and the results are shown in Table 5 and Figure 17.

Table 5. The number of cycles obtained from the EFCs counting method based on grouped dynamic control SOC setpoint using BESS used to deliver DR-LF and DR-HF services with implementing dynamic control for the first 6 EFA blocks for November 2019 frequency data.

	$SOC_{lower}(\%)$								
	10	15	20	25	30	35	40	45	50
$SOC_{higher}(\%)$ 90	2.0559	2.0546	2.0524	2.0493	2.0489	2.0469	2.0454	2.0396	2.0356
85	2.0559	2.0546	2.0524	2.0493	2.0489	2.0469	2.0453	2.0396	2.0357
80	2.0559	2.0546	2.0525	2.0494	2.0489	2.0471	2.0453	2.0396	2.0357
75	2.0557	2.0544	2.0522	2.0492	2.0487	2.0468	2.0452	2.0394	2.0355
70	2.0557	2.0544	2.0522	2.0491	2.0487	2.0468	2.0451	2.0394	2.0355
65	2.0557	2.0544	2.0522	2.0491	2.0487	2.0468	2.0451	2.0394	2.0355
60	2.0551	2.0537	2.0516	2.0485	2.0481	2.0462	2.0445	2.0387	2.0348
55	2.054	2.0533	2.0511	2.0480	2.0476	2.0457	2.0440	2.0383	2.0344
50	2.0526	2.0515	2.0502	2.0478	2.0477	2.0459	2.0444	2.0387	2.0348
45	2.0523	2.0512	2.0498	2.0475	2.0474	2.0456	2.0439	2.0383	2.0383

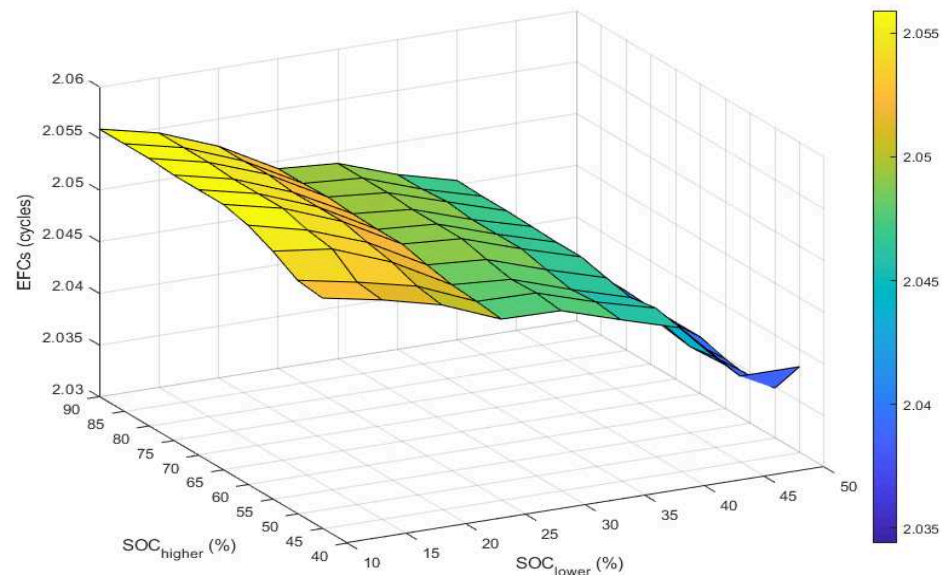


Figure 17. The obtained number of cycles from EFCs for BESS used to deliver DR-HF and DR-LF with Dynamic Control, based on grouped dynamic control SOC setpoint for the first 6 EFA blocks for November 2019 frequency data.

From Table 5 and Figure 17, it can be seen that the number of equivalent full cycles is decreased with the increase in SOC_{lower} and decrease in SOC_{higher} , and vice versa. The highest number of full cycles was at $SOC_{lower} = 10\%$ and $SOC_{higher} = 80\%$, 85% , and 90% , whereas the lowest number of full cycles was at $SOC_{lower} = 50\%$ and $SOC_{higher} = 50\%$. However, based on the results that are obtained from Section 2.11, the availability of BESS in this region was lower compared to the region, which is $SOC_{lower} = 40\%$ and $SOC_{higher} = 45\%$.

When it comes to the revenue, the higher availability is more important than the higher number of full cycles for example; if we have BESS (Li-ion) with a capacity of 40 MWh, a total number of cycles (10,000 cycles), and Purchase Cost (£200/kWh), this value includes the other costs such as battery inverter (£/kW), electrical balancing of the system (BOS) (£/kW), structural balancing of the system (BOS) (£/kW), and operation and maintenance (O & M) (£/kW-yr). The BESS cost per cycle can be calculated using

$$\begin{aligned} \text{Cost per cycle} &= \frac{\text{Cost of BESS } (\text{£/MWh})}{\text{Number of cycles (cycle)}} & (11) \\ &= \frac{\text{£}200/\text{kWh} \times 40 \text{ MWh}}{10,000 \text{ cycle}} = \frac{\text{£}8,000,000}{10,000 \text{ cycle}} \\ &= \text{£}800/\text{cycle} \end{aligned}$$

As we discussed above, the highest number of cycles for the first 6 EFA blocks for November 2019 required 2.0559 cycles; therefore, the cost per cycle/day = £800/cycle × 2.0559 cycle = £1644.72. In case of availability, we assume that the capacity of BESS is still the same as in the above example, and it is used to deliver DR-HF and DR-LF services for the first 6 EFA blocks for November 2019; the DR service price for the year 2022 is £19.37/MW [30], so revenue can be calculated using

$$\begin{aligned} \text{Revenue} &= \text{Contracted Volume (MW)} \times \text{Service} \\ &\quad \text{Price (£/MW/Hour)} \times 24 \text{ Hours} \times \text{Days of month} \quad (12) \end{aligned}$$

$$\begin{aligned} \text{Revenue} &= 40 \text{ MW} \times (\text{£}19.37/\text{MW})/\text{Hour} \times 24 \text{ Hours} \times 1 \\ &= \text{£}18,595.2 \end{aligned}$$

Therefore, based on the obtained results, we can decide that the highest Avg. availability is more important than the highest number of cycles, so the range, which is $SOC_{lower} = 40\%$ and $SOC_{higher} = 45\%$, is considered in this paper when it comes to calculating Avg. availability, number of cycles, and penalty payment.

2.13. Analysis of BESS Used to Deliver DR-LF & DR-HF Services

In this section, each service has been procured for six EFA blocks, and each two EFA blocks have been simulated back-to-back together. Two scenarios have been applied to examine the stacking of both services (DR-LF and DR-HF):

- (S1)—The base case that uses a fixed delay (2 s) and maximum ramp rate;
- (S2)—Using dynamic control, as previously described.

Each pair of EFA blocks has been simulated in MATLAB and, to illustrate the differences between the two scenarios, the SOC_{start} for the stacking of DR-LF and DR-HF are set to different values (30%, 50%, 70%), and the dynamic control setpoints of the SOC are set to ($SOC_{higher} = 45\%$) and ($SOC_{lower} = 40\%$). The results are shown in Tables 6–8 and Figure 18.

Table 6. Simulation results of DR-HF and DR-LF services with the two different scenarios for the first 6 EFA blocks for December 2019 frequency data, $SOC_{start} = 50\%$.

Number of Blocks	SOC_{start} & SOC_{end} (%)	Total Import Energy (MWh)	Total Export Energy (MWh)	Avg. Availability (%)	EFCs	Kj for Each EFA Block	K_e Factor	Scenarios
Block1	50–27.77	−11.63	18.67	100	0.379	0	1	S1
	50–29.06	−11.32	18.17	100	0.373	0	1	S2
Block2	27.77–5.46	−8.93	16.30	99.58	0.315	0	1	S1
	29.06–5.48	−8.87	16.47	99.72	0.334	0	1	S2
Block3	50–49.18	−11.58	10.56	100	0.277	0	1	S1
	50–49.86	−11.22	10.29	100	0.269	0	1	S2
Block4	49.18–70.85	−21.42	10.83	100	0.403	0	1	S1
	49.87–68.73	−19.78	10.78	100	0.382	0	1	S2
Block5	50–53.63	−16.97	13.66	100	0.383	0	1	S1
	50–54.67	−15.71	13.59	100	0.366	0	1	S2
Block6	53.62–57.55	−19.34	15.66	100	0.438	0	1	S1
	54.6–54.85	−18.25	15.57	100	0.423	0	1	S2

Table 7. Simulation results of DR-HF and DR-LF services with the two different scenarios for the first 6 EFA blocks for December 2019 frequency data, $SOC_{start} = 30\%$.

Number of Blocks	SOC_{start} & SOC_{end} (%)	Total Import Energy (MWh)	Total Export Energy (MWh)	Avg. Availability (%)	EFCs	Kj for Each EFA Block	K_e Factor	Scenarios
Block1	30–15.60	−11.63	15.72	98.90	0.342	0	1	S1
	30–15.58	−11.59	15.69	99.14	0.341	0	1	S2
Block2	15.61–5.46	−8.93	11.73	95.89	0.258	0	1	S1
	15.58–5.48	−8.88	11.67	96.78	0.257	0	1	S2
Block3	30–29.18	−11.58	10.56	100	0.277	0	1	S1
	30–31.76	−11.51	9.59	100	0.264	0	1	S2
Block4	29.19–50.85	−21.42	10.83	100	0.403	0	1	S1
	31.77–53.27	−21.31	10.77	100	0.388	0	1	S2
Block5	30–33.63	−16.97	13.66	100	0.383	0	1	S1
	30–34.31	−16.41	13.30	100	0.371	0	1	S2
Block6	33.62–37.55	−19.34	15.66	100	0.4375	0	1	S1
	34.31–39.16	−18.99	15.12	100	0.426	0	1	S2

Table 8. Simulation results of DR-HF and DR-LF services with the two different scenarios for the first 6 EFA blocks for December 2019 frequency data, $SOC_{start} = 70\%$.

Number of Blocks	SOC_{start} & SOC_{end} (%)	Total Import Energy (MWh)	Total Export Energy (MWh)	Avg. Availability (%)	EFCs	Kj for Each EFA Block	K_e Factor	Scenarios
Block1	70–47.77	−11.63	18.67	100	0.379	0	1	S1
	70–44.52	−11.04	18.59	100	0.370	0	1	S2
Block2	47.78–18.64	−8.93	18.87	100	0.348	0	1	S1
	44.53–19.04	−8.55	18.47	100	0.338	0	1	S2
Block3	70–69.18	−11.58	10.56	100	0.277	0	1	S1
	70–67.70	−10.52	10.49	100	0.263	0	1	S2
Block4	69.19–85.13	−18.99	10.83	98.69	0.373	0	1	S1
	67.71–84.76	−19.76	10.78	99.97	0.382	0	1	S2
Block5	70–69.38	−15.17	13.66	97.29	0.360	0	1	S1
	70–69.53	−15.12	13.59	98.90	0.359	0	1	S2
Block6	69.37–73.30	−19.34	15.66	96.01	0.438	0	1	S1
	70–47.77	−18.25	15.57	97.95	0.423	0	1	S2

Figure 18 and Tables 6–8 present the simulation results that are obtained by implementing both DR-LF and DR-HF services for the first six EFA blocks in Dec–2019, based on the two different scenarios (S1&S2). From all these tables, it can be noticed that, in all scenarios, the penalty payment has not occurred at any EFA blocks because the K_e factor is equal to 1, which means that the providers can receive a full payment. In addition to that, the obtained results that are shown in the EFA odd blocks (1, 3, and 5) for all different SOC_{start} illustrate that, at S2, the total export/import energy is minimized over the time compared to S1, and this led to a decrease in the total number of cycles that are obtained from EFCs; the main reason behind this is that the implemented dynamic control has allowed more time for BESS to be charged or discharged. Moreover, from Table 6, the results show that, in all EFA odd blocks when the $SOC_{start} = 50\%$, in both scenarios (S1&S2), the average availability of BESS is 100%, whereas, at the same EFA blocks and for $SOC_{start} = 30\%$, the average availability for BESS reaches 100% for the EFA blocks 3 and 5. However, for EFA block 1 at S1, it is almost 98.90%, and, for S2, it was increased to approximately 99.14%. When $SOC_{start} = 70\%$, the battery reached 100% average availability for both scenarios at EFA blocks (1 and 3), but, for block 5 at (S1), it was $\sim 97.29\%$, and it increased to almost 98.90% for S2.

In the EFA even blocks (2, 4, and 6) for $SOC_{start} = 50\%$, the average availability of BESS reached 100%, except for block 2 (with 99.58% for S1), and it increased to $\sim 99.72\%$. However, for $SOC_{start} = 30\%$, the average availability reached 100% for both S1 and S2 for EFA blocks (4 and 6), but, for block 2, it equates to 95.89% for S1, and it increased to approximately 96.78%. For $SOC_{start} = 70\%$, BESS reached 100% average availability at only EFA block 2, and the main reason why BESS did not reach 100% average availability for the first and second EFA blocks, although a dynamic control had been applied, is that the battery reached $SOC_{lower} = 5\%$, which made it unavailable for a certain time.

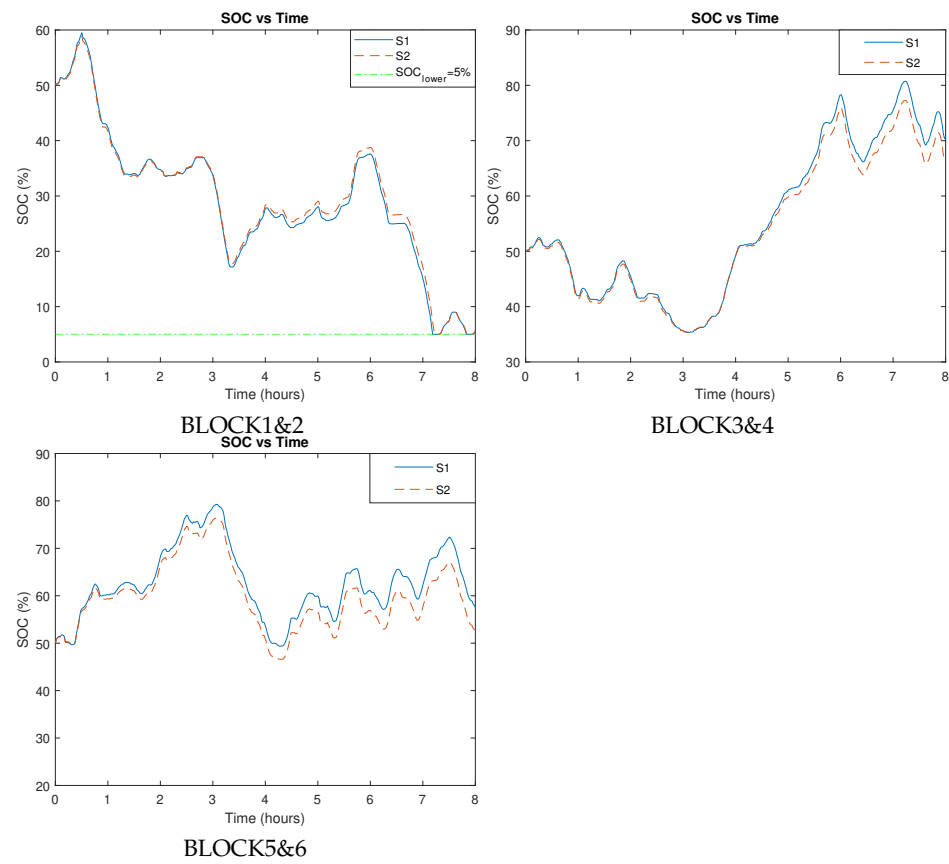


Figure 18. Simulation results for battery SOC for different scenarios (S1 and S2) for the first six EFA blocks of December 2019 frequency data, $SOC_{start} = 50\%$.

3. Conclusions

The analysis of Battery Energy Storage Systems for delivering both DR-LF and DR-HF services has provided valuable insights into the dynamic control strategies and performance metrics of these systems. The study explored various scenarios, including fixed delay (S1) and dynamic control (S2) for SOC management. The findings reveal that the dynamic control strategy (S2) significantly improved the overall performance of BESS by minimizing the total import/export energy and the number of equivalent full cycles (EFCs). This reduction in energy throughput and EFCs indicates the potential for extending the operational life and reliability of the BESS, while still meeting the service demands effectively.

Furthermore, the analysis emphasized the importance of BESS availability, where a higher average availability of the system was considered more crucial than achieving a higher number of cycles. This is particularly relevant when considering the economics of BESS deployment and the associated cost per cycle. Overall, the study underscores the significance of dynamic control strategies in optimizing BESS performance for DR-LF and DR-HF services. These insights can be beneficial for decision-makers and stakeholders in the energy sector seeking to implement efficient and cost-effective energy storage solutions while enhancing grid stability and reliability.

Author Contributions: Conceptualization, D.T.G.; Investigation, A.A.; Methodology, A.A.; Supervision, D.T.G.; Writing—original draft, A.A.; Writing—review and editing, D.T.G. All authors have read and agreed to the published version of the manuscript.

Funding: This research was funded by the Embassy of the Libyan Arab Republic in London: BT/LN/299102400418.

Data Availability Statement: Data supporting this systematic review are available in the reference section. In addition, the analyzed data that were used during the current systematic review are available from the author on reasonable request.

Conflicts of Interest: The authors declare no conflict of interest.

References

1. Strbac, G.; Aunedi, M.; Pudjianto, D.; Djapic, P.; Teng, F.; Sturt, A.; Jackravut, D.; Sansom, R.; Yufit, V.; Brandon, N. Strategic assessment of the role and value of energy storage systems in the UK low carbon energy future. In *Report for Carbon Trust*; Imperial College London: London, UK, 2012.
2. Mehr, T.H.; Masoum, M.A.; Jabalameli, N. Grid-connected Lithium-ion battery energy storage system for load leveling and peak shaving. In Proceedings of the 2013 Australasian Universities Power Engineering Conference (AUPEC), Hobart, TAS, Australia, 29 September–3 October 2013; pp. 1–6.
3. Liang, X. Emerging power quality challenges due to integration of renewable energy sources. *IEEE Trans. Ind. Appl.* **2016**, *53*, 855–866. [[CrossRef](#)]
4. Kundur, P.S.; Malik, O.P. *Power System Stability and Control*; McGraw-Hill Education: New York, NY, USA, 2022.
5. Gil, G.O.; Chowdhury, J.I.; Balta-Ozkan, N.; Hu, Y.; Varga, L.; Hart, P. Optimising renewable energy integration in new housing developments with low carbon technologies. *Renew. Energy* **2021**, *169*, 527–540. [[CrossRef](#)]
6. Vazquez, S.; Lukic, S.M.; Galvan, E.; Franquelo, L.G.; Carrasco, J.M. Energy storage systems for transport and grid applications. *IEEE Trans. Ind. Electron.* **2010**, *57*, 3881–3895. [[CrossRef](#)]
7. Diehl, A. Why is Energy Storage Such an Important Part of the Renewables Mix. 2015. Available online: <https://www.civicsolar.com/article/why-energy-storage-such-important-part-renewables-mix> (accessed on 8 March 2022).
8. Tan, K.M.; Babu, T.S.; Ramachandaramurthy, V.K.; Kasinathan, P.; Solanki, S.G.; Raveendran, S.K. Empowering smart grid: A comprehensive review of energy storage technology and application with renewable energy integration. *J. Energy Storage* **2021**, *39*, 102591. [[CrossRef](#)]
9. Niroomand, M.; Feldmann, T.; Bollin, E. High-performance control system for grid-tied ESSs. *IET Gener. Transm. Distrib.* **2017**, *11*, 2138–2145. [[CrossRef](#)]
10. Divya, K.; Østergaard, J. Battery energy storage technology for power systems—An overview. *Electr. Power Syst. Res.* **2009**, *79*, 511–520. [[CrossRef](#)]
11. Rana, M.M.; Uddin, M.; Sarkar, M.R.; Meraj, S.T.; Shafiullah, G.; Muyeen, S.; Islam, M.A.; Jamal, T. Applications of energy storage systems in power grids with and without renewable energy integration—A comprehensive review. *J. Energy Storage* **2023**, *68*, 107811. [[CrossRef](#)]
12. Ciez, R.E.; Whitacre, J. Comparative techno-economic analysis of hybrid micro-grid systems utilizing different battery types. *Energy Convers. Manag.* **2016**, *112*, 435–444. [[CrossRef](#)]
13. Yadlapalli, R.T.; Alla, R.R.; Kandipati, R.; Kotapati, A. Super capacitors for energy storage: Progress, applications and challenges. *J. Energy Storage* **2022**, *49*, 104194. [[CrossRef](#)]
14. Rayit, N.S.; Chowdhury, J.I.; Balta-Ozkan, N. Techno-economic optimisation of battery storage for grid-level energy services using curtailed energy from wind. *J. Energy Storage* **2021**, *39*, 102641. [[CrossRef](#)]
15. Gundogdu, B.M.; Nejad, S.; Gladwin, D.T.; Foster, M.P.; Stone, D.A. A battery energy management strategy for UK enhanced frequency response and triad avoidance. *IEEE Trans. Ind. Electron.* **2018**, *65*, 9509–9517. [[CrossRef](#)]
16. Shaqsi, A.Z.A.; Sopian, K.; Al-Hinai, A. Review of energy storage services, applications, limitations, and benefits. *Energy Rep.* **2020**, *6*, 288–306. [[CrossRef](#)]
17. Xu, X.; Bishop, M.; Oikarinen, D.G.; Hao, C. Application and modeling of battery energy storage in power systems. *CSEE J. Power Energy Syst.* **2016**, *2*, 82–90. [[CrossRef](#)]
18. Song, Z.; Nazir, M.S.; Cui, X.; Hiskens, I.A.; Hofmann, H. Benefit assessment of second-life electric vehicle lithium-ion batteries in distributed power grid applications. *J. Energy Storage* **2022**, *56*, 105939. [[CrossRef](#)]
19. Gundogdu, B.; Gladwin, D.; Stone, D. Battery energy management strategies for UK firm frequency response services and energy arbitrage. *J. Eng.* **2019**, *2019*, 4152–4157. [[CrossRef](#)]
20. National grid ESO. *Future of Frequency Response, 2021*; National Grid ESO: Warwick, UK, 2017.
21. NGESO. EBR Article 18 Response consultation Terms and Conditions. 2022. Available online: <https://www.nationalgrideso.com/calendar/ebr-article-18-response-consultation-terms-and-conditions> (accessed on 15 December 2022).
22. National Grid ESO. Historic Frequency Data. 2021. Available online: <https://www.nationalgrideso.com/industry-information/balancing-services/frequency-response-services/historic-frequency-data> (accessed on 8 March 2022).
23. National Grid ESO. Dynamic Regulation-Technical Requirements. 2022. Available online: <https://www.nationalgrideso.com/industry-information/balancing-services/Frequency-Response-Services/Dynamic-Regulation/Technical-Requirements> (accessed on 18 October 2022).
24. Guo, W.; Bai, H.; Szatmari-Voicu, G.; Taylor, A.; Patterson, J.; Kane, J. A 10kW 97%-efficiency LLC resonant DC/DC converter with wide range of output voltage for the battery chargers in Plug-in Hybrid Electric Vehicles. In Proceedings of the 2012 IEEE Transportation Electrification Conference and Expo (ITEC), Dearborn, MI, USA, 18–20 June 2012; pp. 1–4.

25. Qian, H.; Zhang, J.; Lai, J.S.; Yu, W. A high-efficiency grid-tie battery energy storage system. *IEEE Trans. Power Electron.* **2010**, *26*, 886–896. [[CrossRef](#)]
26. Abdulkarim, A.; Gladwin, D.T. A sensitivity analysis on power to energy ratios for energy storage systems providing both dynamic firm and dynamic containment frequency response services in the uk. In Proceedings of the IECON 2021–2047th Annual Conference of the IEEE Industrial Electronics Society, Toronto, ON, Canada, 13–16 October 2021; pp. 1–6.
27. Energy Storage. Every Charge Cycle Counts When It Comes to Battery Degradation. 2021. Available online: <https://www.energy-storage.news/blogs/every-charge-cycle-counts-when-it-comes-to-battery-degradation> (accessed on 8 September 2021).
28. National Grid ESO. Simplification and Standardisation of FFR Service. 2018. Available online: <https://www.nationalgrideso.com/document/102071/download> (accessed on 6 January 2023).
29. Abdulkarim, A.; Gladwin, D.T. Maximizing energy availability for a Dynamic Regulation Frequency Response Service for Battery Energy Storage Systems. In Proceedings of the IECON 2022–2048th Annual Conference of the IEEE Industrial Electronics Society, Brussels, Belgium, 17–20 October 2022; pp. 1–6.
30. MODO. Reference Price. 2022. Available online: <https://platform.modo.energy/home> (accessed on 16 January 2023).

Disclaimer/Publisher’s Note: The statements, opinions and data contained in all publications are solely those of the individual author(s) and contributor(s) and not of MDPI and/or the editor(s). MDPI and/or the editor(s) disclaim responsibility for any injury to people or property resulting from any ideas, methods, instructions or products referred to in the content.